Journal of Glaciology

Article

Cite this article: Zhou C, Liu Y, Zheng L (2022). Satellite-derived dry-snow line as an indicator of the local climate on the Antarctic Peninsula. *Journal of Glaciology* **68**(267), 54–64. https://doi.org/10.1017/jog.2021.72

Received: 18 November 2020
Revised: 1 June 2021
Accepted: 1 June 2021
First published online: 25 June 2021

Key words:
Antarctic Peninsula; dry-snow line; glacial zones; SAR

Author for correspondence:
Chunxia Zhou,
E-mail: zhoucx@whu.edu.cn

Satellite-derived dry-snow line as an indicator of the local climate on the Antarctic Peninsula

Chunxia Zhou, Yong Liu and Lei Zheng

Chinese Antarctic Center of Surveying and Mapping, Wuhan University, Wuhan 430079, China

Abstract

Recent regional cooling has impacted the natural systems of the Antarctic Peninsula (AP); however, little is known concerning the changes in the high parts of the glacial systems. Dry-snow line (DSL), situated in the high parts of glaciers, is the uppermost limit of frequent or occasional surface melt. We analyse dry-snow line altitude (DSLA) changes on the AP during 2004–2020 using C-band synthetic aperture radar time series data. We demonstrate that the DSLA in the eastern part of the AP is usually higher than that of the western part. Moreover, using simulated climatic variables from regional climate models, the lowering in altitude of DSL of glaciers in most areas is identified as a response to a decrease in snowmelt and an increase in precipitation. Furthermore, correlation analyses between simulated climatic variables and the DSLA are conducted. These results present the sensitive response of variations in DSLA to meteorological conditions, and the capability of DSLA being a proxy of polar local climate in high-altitude areas with no in situ meteorological observations.

1. Introduction

Over the second half of the last century, the Antarctic Peninsula (AP) has witnessed pronounced regional warming (2.5–3 K) (Vaughan and others, 2003; Turner and others, 2005), which is one of the largest warming rates on earth (Oliva and others, 2017; Costi and others, 2018). Since 1999, several studies indicate that regional cooling ($-0.47\ \mathrm{K\ decade^{-1}}$) has occurred on the AP (Turner and others, 2016; Oliva and others, 2017). As a consequence, the regional cooling trend has impacted on the natural systems of the AP, including (1) decreases in summer snowmelt and meltwater production (van Wessem and others, 2015; Bevan and others, 2018; Datta and others, 2018; Zheng and others, 2019), (2) decelerating recession of glaciers (Oliva and others, 2017), (3) thinning of permafrost active layer (Hrbáček and others, 2016; Sancho and others, 2017) and (4) reduction in sea-level contribution by peripheral glaciers (Hock and others, 2009; Gardner and others, 2013; Oliva and others, 2017). However, the long-term trend of surface-air temperature of the AP for more than 60 years is one of warming (Bromwich and Nicolas, 2014). Argentina's Esperanza research station, on the very northern tip of the AP, reached a record high surface-air temperature of 18.3°C in 2020 (Dwyer, 2020). Moreover, enhanced winter snowmelt has endangered the ice shelves on the AP (Zheng and others, 2020). With the background of changing climate, little is known concerning the changes in the higher parts of glacial systems over the past two decades.

The evolution of glacial zones is closely related to the variations in climatic variables. Glacial zones primarily comprise the dry-snow zone (DSZ), frozen percolation zone, wet-snow zone and bare ice zone (Benson, 1961; Paterson, 1994). The DSZ is restricted to the uppermost part of glaciers and does not melt for a whole year (Rau and others, 2000*b*; Arigony-Neto and others, 2009; Huang and others, 2013). Subjected to freeze–thaw cycles, the frozen percolation zone skirting the DSZ is characterised by large grain sizes and numerous subsurface ice bodies (Rau and others, 2000*b*). In the wet-snow zone, melt events lead to the increase of liquid water content in the snowpack. The bare ice zone is situated on the lowest areas of glaciers where the entire annual accumulation of snow melts, exposing bare ice at the surface (Huang and others, 2013). The lower boundary of the DSZ is referred to as the dry-snow line (DSL), which is the upper bound of the summer snowmelt and separates the DSZ and the frozen percolation zone. The DSL in the high parts of glacial systems can be an indicator of climate change due to its high sensitivity to local and regional climatic variables (Rau and others, 2000*b*). In situ measurements are hampered by steep mountainous terrain and severe weather conditions, and remote-sensing data thus provide an impactful tool to monitor changes in high altitudes and latitudes with a variety of spatial and temporal resolutions. In polar regions, spaceborne synthetic aperture radar (SAR) is particularly helpful because of its advantage of insensitivity to solar illumination and atmospheric conditions. Several studies have demonstrated the suitability of SAR images for mapping glacier zones in glacial areas (Rau and others, 2000*b*; Huang and others, 2011; Zhou and Zheng, 2017).

Radar backscatter from snow cover and glacier surfaces depend on the liquid water content, grain size, snow density, stratigraphy and surface roughness in SAR images (Benson, 1961; Rau, 2002). Due to the fine grain size and low liquid water content, even dry snowpacks with a thickness of several meters appear transparent in SAR images, and the high penetration depth and predominant volume scattering lead to the presence of dark signatures in the DSZ (low backscatter values) in SAR images (Ulaby and others, 1983; Rau and others, 2000*a*). By comparison,

Table 1. Specifications of SAR sensors used in this study

Platform	Sensor	Mode	Resolution (m)	Polarisation	Year	Number
Envisat	ASAR	Image	30	HH	2004–2010	283
		Wide Swath	150	HH	2011	6
RADARSAT-2	SAR	ScanSAR Wide	100	HH	2012–2013	5
Sentinel-1A/B	SAR	Extra Wide Swath	40	HH	2014–2020	61

snowpacks in the frozen percolation zone at the end of the summer, which are characterised by coarse grain and cluster sizes, abundant ice layers and pipes and high densities, show bright signatures (high backscatter values) in SAR images (Rau and others, 2000*b*). The wet-snow zone presents dark signatures similar to DSZ because of the strong absorption of radar signals and scattering on smooth surfaces (Rau and others, 2000*b*). Surface scattering in the bare ice zone causes relatively high backscatter values when compared with that of the wet-snow zone. Therefore, SAR images of glaciers show a typical sequence of alternating dark and bright signatures. The DSL can be extracted from SAR images on the basis of differences in glacial zones by using various methods, such as the thresholding method (Rau, 2002), decision tree (Arigony-Neto and others, 2006; Zhou and Zheng, 2017) and support vector machines (Huang and others, 2011).

Quantitative analysis of dry-snow line altitude (DSLA) changes and the response of DSLA to climate change is important. The position of the DSL is generally stable, and only severe snowmelt caused by rising temperatures can shift it upward. Conversely, a downward shift indicates the continuous accumulation of fine snow without melting metamorphism (Rau and others, 2000*b*; Rau, 2002; Rau and Braun, 2002). Accordingly, the change of the DSLA is a reflection of climate change at the high parts of glacial systems. Several studies have focused on the time series variations in the DSLA on the AP. Rau (2002) revealed the increase in the DSLA on the eastern AP between 65°S and 68°S during 1991–2000. Rau and Braun (2002) followed with interest the DSLA on the AP north of 70°S using ERS-1/2 SAR images between 1992 and 2000. Arigony-Neto and others (2007) utilised a 'centreline approach' on the basis of ERS-1/2 SAR and Envisat ASAR data to explore the variations in the DSLA on the Detroit Plateau and Marguerite Bay of the AP. Arigony-Neto and others (2009) subsequently investigated time series changes (1992–2005) in DSLA on the AP north of 70°S. However, these studies focused on regional changes in the DSLA (Rau, 2002; Arigony-Neto and others, 2007) on the AP north of 70°S (Rau and Braun, 2002; Arigony-Neto and others, 2009) but no information was provided on the AP south of 70°S. Although the 'centreline approach' method used in the time series analysis can simplify the detection of the DSL (Arigony-Neto and others, 2006, 2007, 2009), it fails to reflect the status of the whole glacier. The altitude of the change point on the axis of the glacier is sometimes inconsistent with the mean DSLA because the DSL is curved (Huang and others, 2012). Furthermore, previous studies only qualitatively analysed the relationship between meteorological conditions and DSLA and research on quantitative relationships between them are limited.

Adequate remote-sensing and auxiliary data facilitate time series analyses of DSLA changes. We analysed spatiotemporal variations in the DSLA on the AP based on multisensor C-band SAR data (Envisat, RADARSAT-2 and Sentinel-1A/B) to monitor the response of DSLA to the shifting climate and fill the gaps in the study of DSLA changes from 2005 to 2020. Correlation analyses between climatic variables and the DSLA were conducted. The remainder of this paper is organised as follows. The study area and dataset are introduced in Section 2. Data processing and analytical methods are presented in Section 3. Annual changes and trends in the DSLA are given in Section 4, followed by a discussion in Section 5. Lastly, the conclusions of this study are drawn in Section 6.

2. Data set

2.1 SAR images

Time series of C-band SAR images from Envisat, RADARSAT-2 and Sentinel-1A/B covering the period of 2005–2020 were adopted in this study. SAR data consisting of 355 images of HH polarisation acquired in descending or ascending orbit (Table 1) were used to derive the DSL. SAR data for extracting DSL are best obtained after the ablation season to minimise the impact of ongoing snowmelt on DSL. Furthermore, to capture the continuous melt seasons to facilitate the correlation analyses between the climatic variables and DSLA, the majority of the SAR data used in this study were collected in early austral winter when snow accumulation has little effect on DSL. The period from May of the previous year to April of the next year was regarded as the balance year. The DSL derived from the SAR data reflects the condition of the whole balance year. Filenames of SAR data are listed in Table S1 of Supplementary Materials.

The main steps of data preprocessing conducted with the Sentinel Application Platform (SNAP) from the European Space Agency (ESA) include radiometric calibration, range-Doppler terrain correction, speckle filtering and SAR mosaicking. Radiometric calibration can provide images in which pixel values can be directly related to the radar backscatter of the scene. Terrain corrections were applied using the Reference Elevation Model of Antarctica digital surface model (REMA DSM) at a resolution of 200 m to compensate for the distortions caused by topographical variations and oblique satellite sensors. To reduce the speckle effect, a 7×7 Lee filter was applied. A cosine radiometric correction (Mladenova and others, 2013; Topouzelis and Singha, 2016) was then used to compensate for σ^0 range variations caused by the changing incidence angle with distance according to:

$$\sigma^0_{\mathrm{nor}} = \frac{\sigma^0_\theta \cos^2(\theta_{\mathrm{nor}})}{\cos^2(\theta)}, \quad (1)$$

where σ^0_{nor} is the normalised backscatter value, θ is the local incidence angle, σ^0_θ represents the original backscatter value and θ_{nor} indicates the normalised angle, which was set to 30° in this study. Lastly, overlapping images were mosaicked as a composite image.

2.2 Regional atmospheric climate model

The regional atmospheric climate model RACMO2.3 combines the dynamics package of the High Resolution Limited Area Model (HIRLAM) (Undén and others, 2002) with the physics package of the European Centre for Medium-range Weather Forecasts (ECMWF) Integrated Forecast System (IFS) (Ecmwf, 2009). The RACMO2.3p2 Antarctic Peninsula model (hereafter, 'RACMO') has a horizontal resolution of 5.5 km in terms of the surface mass balance (SMB) and its components (e.g. precipitation, snowmelt and sublimation) for 1979–2019 (van Wessem

https://doi.org/10.1017/jog.2021.72 Published online by Cambridge University Press

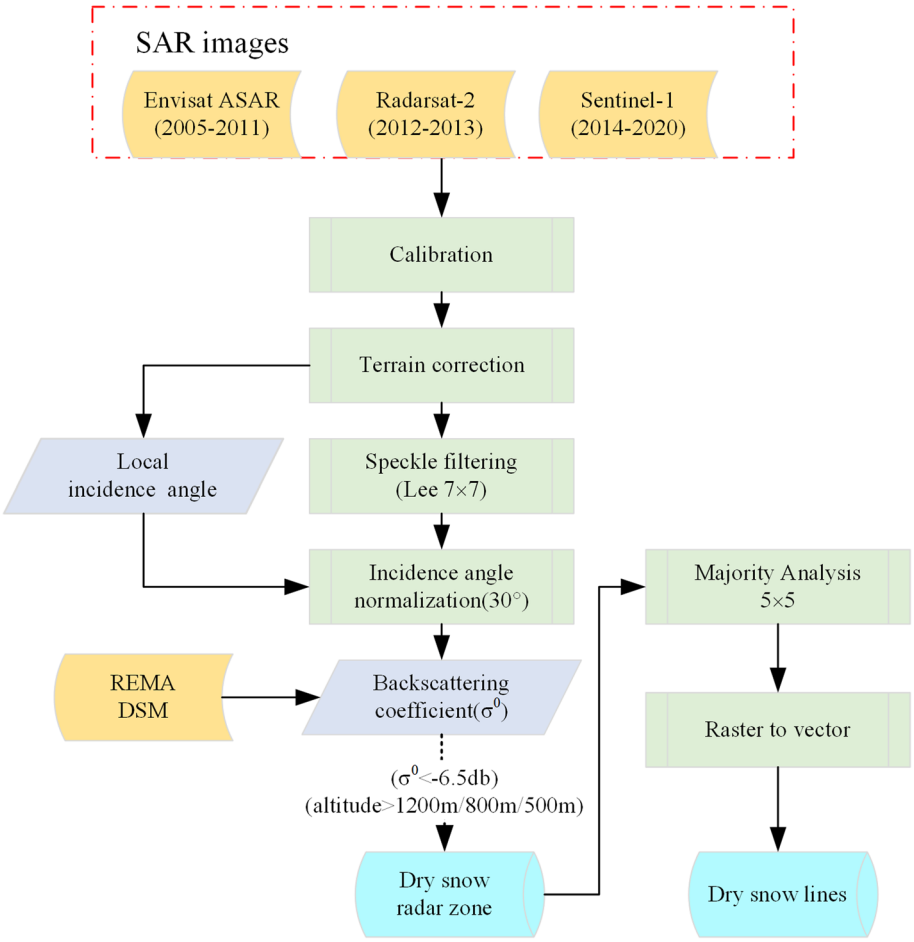

Fig. 1. Flowchart for DSL extraction with SAR images.

and others, 2016, 2018). We utilised the RACMO model to analyse the correlation between DSLA changes and simulated climatic variables on the AP from the balance year 2004/05 to 2018/19.

3. Methods

The DSZ can be distinguished from other zones due to the difference in backscattering characteristics and altitude. A thresholding method was adopted in this study to map the DSZ and extract the DSL. On the basis of the MEMLS3&a (an extension of the Microwave Emission Model of Layered Snowpacks) (Proksch and others, 2015), Zhou and Zheng (2017) simulated C-band σ^0 changes in transitions from dry to wet snow regimes. When the incidence angle was set to 30° in the simulation, Zhou and Zheng (2017) found that σ^0 of coarse-grained snowpacks increases above −6.5 dB rapidly while maintaining it below −6.5 dB in fine-grained snowpacks with the increase of the snow depth. Fine- and coarse-grained snowpacks correspond to the frozen percolation zone and DSZ after the ablation season, respectively, while changes in density only contribute to a minor degree of backscatter values (Rau and others, 2000*b*). The frozen percolation zone that experiences melting events in summer leads to backscatter values increasing rapidly above −6.5 dB in winter, while σ^0 remains below −6.5 dB in the DSZ. It is noteworthy that although accumulation of fine snow over areas of the frozen percolation can decrease backscatter values, it is not significant. Therefore, it is a reasonable threshold to differentiate between the frozen percolation zone ($\sigma^0 \geq -6.5$ dB) and DSZ ($\sigma^0 < -6.5$ dB) after the ablation season when using C-band SAR images normalised to an incidence angle of 30°. Zhou and Zheng (2017) applied this threshold successfully and the DSZ detected by $\sigma^0 < -6.5$ dB is consistent with on-melt areas derived from microwave radiometers.

Altitude is also an important condition for differentiating glacial zones. The DSZ is restricted to the uppermost part of glaciers and the DSL is considered coincident with the −11°C isotherm of the mean annual air temperature (Peel, 1992), while the wet-snow zone is lower than the isotherm of −11°C. An altitude lower than 500 m is deemed to be bare ice (Rau, 2002; Arigony-Neto and others, 2007).To distinguish the DSZ from the wet-snow zone and bare ice zone with analogous backscattering characteristics, altitude is thereby the other threshold considered for extracting DSL. Arigony-Neto and others (2009) reported that the DSL occurs only above 1200 m (in areas north of 67.5°S) and 800 m (in areas between 67.5°S and 72°S) on the AP. Considering that surface air temperature decreases with increasing latitude, 800 m is no longer applicable to approximate the −11°C isotherm in areas south of 72° S, and 500 m is chosen as a suitable value. Consequently, a restraining threshold of 1200, 800 and 500 m was adopted in areas north of 67.5°S, between 67.5°S and 72°S and south of 72°S, respectively. Altitude information was derived from the REMA DSM at a resolution of 200 m (https://www.pgc.umn.edu/data/rema/) (Howat and others, 2019). The flowchart for SAR image preprocessing, DSZ detection and DSL extraction is shown in Figure 1.

Majority analysis can change spurious pixels to the class that the majority of the pixels in a $n \times n$ kernel has. To reduce misclassification, a majority analysis of 5×5 windows was conducted using Environment for Visualising Images (ENVI) after detecting the DSZ. Lastly, the DSL was extracted via the raster-to-vector operation.

Geometric and inherent distortions (e.g. layover and foreshortening) are severe in SAR images due to the complex topography of the AP. To reduce classification mistakes caused by geometric distortions, we chose glaciers with widths larger than 1000 m,

https://doi.org/10.1017/jog.2021.72 Published online by Cambridge University Press

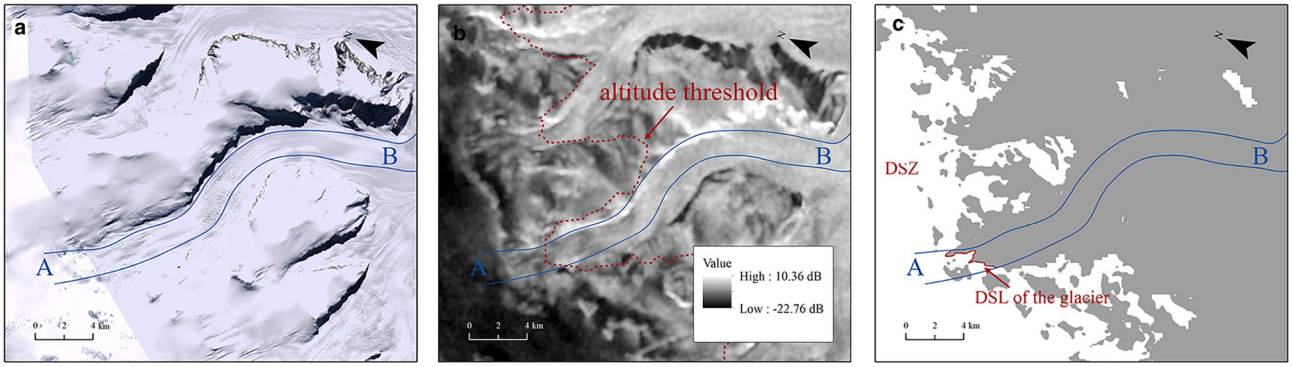

Fig. 2. DSL detection of the Breitfuss Glacier (66.97°S, 64.87°W). (a) Subset of the Landsat Image Mosaic of Antarctica (LIMA; link: https://lima.usgs.gov/access.php) (Bindschadler and others, 2008). (b) Subset of the Sentinel-1B SAR images acquired on 2 May 2019. (c) DSZ classification. The blue line denotes the edge line of the glacier that flows from A to B. White and grey areas in (c) represent DSZ and other zones, respectively. The red line in (c) represents the DSL of the Breitfuss Glacier.

analysed the part of glacial surfaces far from steep ridges instead of entire glacial surfaces. As shown in Figure 2, we limited the study area between glacier edge lines. In this way, the section where the lower boundary of the DSZ intersects two edge lines was considered the DSL of the glacier (Fig. 2c). The mean altitude of the DSL was treated as the DSLA of the glacier. The mean DSLA for different sectors divided by latitude was obtained by the width weighted average of the mean DSLA of all glaciers in the sector.

The total annual precipitation, snowmelt and SMB, calculated as the summation of the corresponding variable in a mass-balance year within a given sector, were analysed to assess changes of simulated climate. Precipitation and snowmelt anomalies were computed as the ratio of departures of total annual values to mean total annual values in a given sector from 2004/05 to 2018/19 and expressed as a percentage. All statistics based on RACMO were only in the Graham Land and Palmer Land on the AP, while the ice shelves were masked.

4. Results

4.1 Spatial extent of the DSL

The spatial extent of the DSZ on the AP (excluding Alexander Island) was identified (Fig. 3). The DSL derived from different SAR sensors indicates that the threshold method is suitable for mapping the DSL on the AP because it consistently demarcates dark areas (low backscatter values) in mountainous regions of the AP. Abnormal intense winter snowmelt was observed in 2015/2016 on the AP (Zheng and others, 2020), and the adoption of an altitude threshold appropriately distinguishes DSZ and the wet-snow zone with analogous backscattering characteristics (Fig. 3b).

The glacier edge-line method was used to investigate 227 glaciers, with 104 glaciers located on the east side and 123 glaciers situated on the west side of the AP. The spatial distribution of the mean DSLA detected for the balance year 2017/18 is presented in Figure 4a. Mean values of DSLA on the west and east side are 1037 ± 324 and 929 ± 200 m, respectively. Moreover, on both sides of the AP, mean DSLA of each sector decreases from north to south due to the reduction in snowmelt as controlled by the decrease of temperature from low to high latitudes. A histogram of the mean DSLA distribution (Fig. 4b) shows that the mean DSLA on the east side of the AP is distributed at 800–1900 m, while the mean DSLA on the west side is distributed at 500–1900 m. Compared to those on the west side, more glaciers with DSLA higher than 1500 m are located on the east side. Furthermore, 81 out of 104 glaciers on the east side show a mean DSLA higher than 1200 m, while the mean DSLA of 92 out of 123 glaciers on the west side is between 1100 and 1600 m. The mean DSLA and distribution curves show that DSLA on the east side is generally higher than that on the west side.

4.2 DSLA interannual variations

Interannual variations in the DSLA were identified on both sides of the AP from 2004/05 to 2019/20 (Figs 5, 6), and precipitation and snowmelt anomalies were computed in each sector from 2004/05 to 2018/19 (the sector north of 64°S refers to the region between 63.75°S and 64°S as the DSL in the areas north of 63.75°S is not present). Annual changes in DSLA show various regional patterns. On the east side of the AP, similar variations of DSLA in regions north of 69°S typically decreased from 2004/05 to 2010/11 (Figs 5a, c–e), increased and then decreased again to a local low in 2018/19, followed by an upward variation in 2019/20. DSLA in the south-eastern AP generally remained stable from 2004/05 to 2009/10 (Figs 5g, j–k), reached a minimum in 2010/11 or 2011/12 (Figs 5g–j) and then showed an increasing trend (Figs 5g–i).

DSLA is determined by snowmelt and precipitation. Severe snowmelt caused by rising temperatures can shift DSL upwards, whereas a downward shift indicates continuous accumulation of fine snow without the melting metamorphism (Rau and others, 2000*b*; Rau, 2002; Rau and Braun, 2002). The DSLA in many sectors experienced increases relative to the previous year during the balance year of intense snowmelt in 2005/06 (Figs 5a, b, g–j). Additional details are provided when the annual snowmelt is mapped (Fig. S1). Although the total annual snowmelt in 2005/06 is higher than that in 2004/05, large-scale melting in 2004/05 even reached central plateaus of the AP (Fig. S1a). Large snowmelt anomalies in 2012/13 also caused some increasing events (Figs 5g–j). Moreover, the declining DSLA in 2010/11 can be attributed to positive precipitation anomalies (Figs 5a–b, d–g, i, j) without high positive snowmelt anomalies. Additional details are presented in Figure S2g, and nearly all sectors experienced an increase in precipitation in 2010/11.

DSLA remained steady between 64°S and 69°S (Figs 6b–f), while sectors south of 69°S showed a clear downward trend (Figs 6g–k) on the west side of the AP. The DSLA is high (Figs 6a–b) in balance years 2004/05 and 2005/06 when the snowmelt is intense (Figs S1a, b), and changes in DSLA were similar to those of snowmelt (Figs 6a–d, g–i). Similar to the east side, low DSLA in some sectors occurred in 2010/11 (Figs 6h–j). The DSLA showed a decreasing trend (Figs 6a–g, i–k) when melting decreases significantly from 2006/07 to 2007/08, and this pattern would have been more pronounced if it had been accompanied by an increase in precipitation. However, intense melting was accompanied by high precipitation anomalies in the balance year 2016/17, and changes in DSLA relative to the previous year were uncertain (Figs 6b–k).

The RACMO model between 2004/05 and 2018/19 indicates that the total annual snowmelt is relatively similar over both the

https://doi.org/10.1017/jog.2021.72 Published online by Cambridge University Press

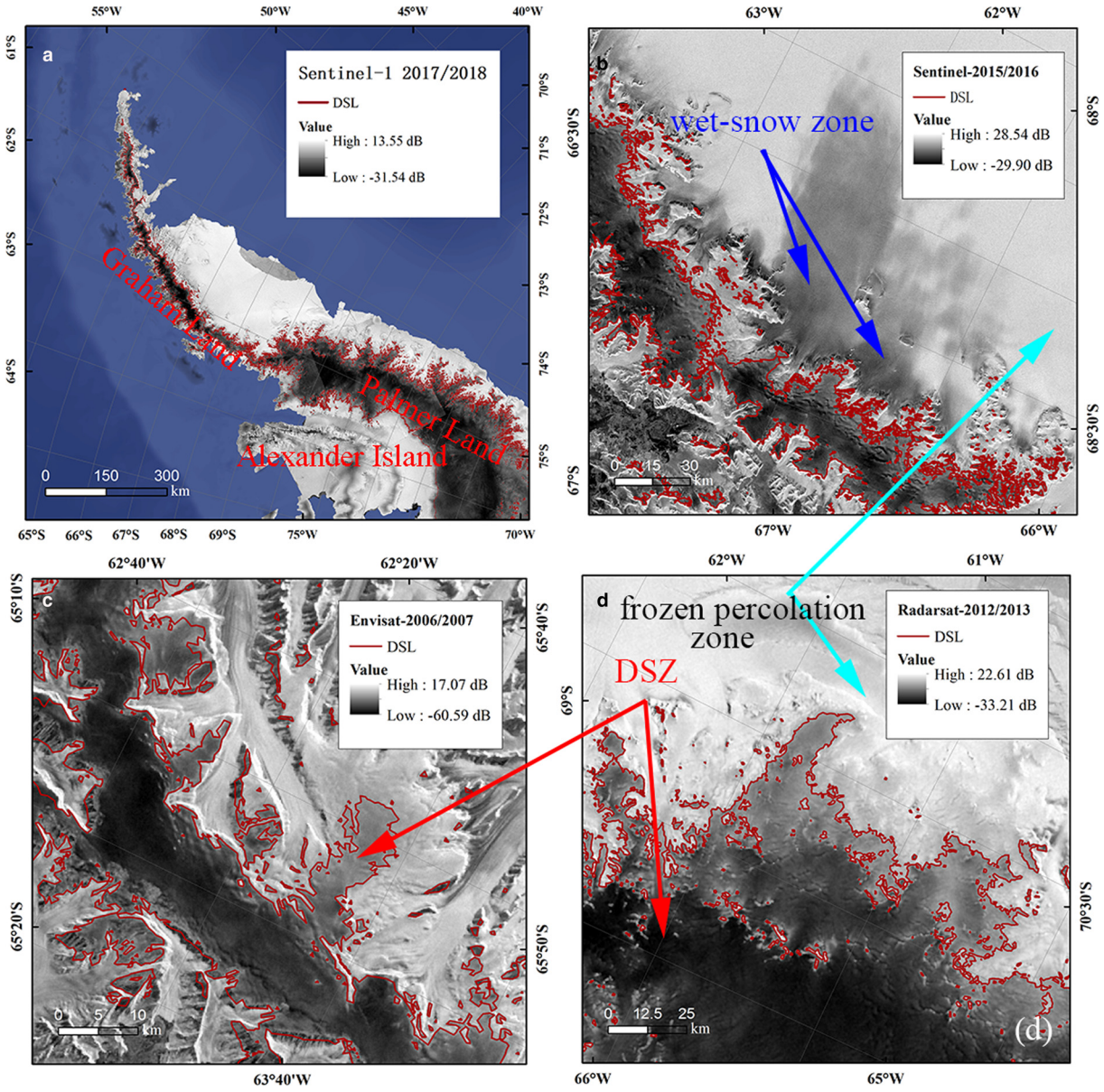

Fig. 3. Mapping of the DSL. Spatial distribution of the DSL on the AP in the balance year of (a) 2017/18 derived from Sentinel-1 A/B, (b) 2015/16 from Sentinel-1 A/B, (c) 2006/07 from Envisat and (d) 2012/13 from Radarsat-2.

west and east sides of the AP (Tables 2, 3). However, the total annual precipitation on the west side of the AP is significantly higher than that on the east side (Tables 2, 3). The total annual snowmelt shows negative trends in the grounded ice sheet of the AP, and precipitation exhibits positive trends in nearly all sectors on both sides (Tables 2, 3). DSLA manifests a downtrend in most sectors, especially in the southern part of AP (Tables 2, 3), due to the decreased snowmelt and increased precipitation. DSLA shows an increasing trend in these sectors at 64°S/65°S, 67°S/68°S and 68°S/69°S on the west side (Table 2) and 64°S/65°S and 67°S/68°S on the east side (Table 3). Among them, the DSL in sector 64°S/65°S on the west side of AP has experienced the most significant upward migration (Table 2).

4.3 Responses of DSLA to climate variables

Correlation analyses between simulated climatic variables and the DSLA were conducted (Figs 7, 8). The correlation between the total annual precipitation is insignificant while the logarithmic relationship between the total annual snowmelt and DSLA is fitted and the goodness of fit R^2 reaches 0.67 on the east side of the AP (Fig. 7). Similar to the east side, the logarithmic total annual snowmelt–DSLA relationship is fitted on the west side (Fig. 8a). The relationship between total annual precipitation and DSLA is complex (Fig. 8b). With the increase of total annual precipitation, DSLA shows a decreasing trend at the beginning, but when it reaches $\sim 5 \times 10^5$ mm w.e., DSLA begins to increase and then remains stable after the total annual precipitation is $>10 \times 10^5$ mm w.e. (Fig. 8b). The correlation analyses demonstrate that the DSLA responds to climate and can therefore be used as an indicator of climate change.

5. Discussion

5.1 Different DSLA patterns on the west and east sides

DSLA shows remarkable differences on both sides of the AP. The mean DSLA in nearly all sectors at the same latitude is higher on the east side (Fig. 4a), and more glaciers with DSLA higher than 1500 m are located on the east side when compared with those of the west side (Fig. 4b). This result is different from that found by Arigony-Neto and others (2009), who concluded that the DSLA is

https://doi.org/10.1017/jog.2021.72 Published online by Cambridge University Press

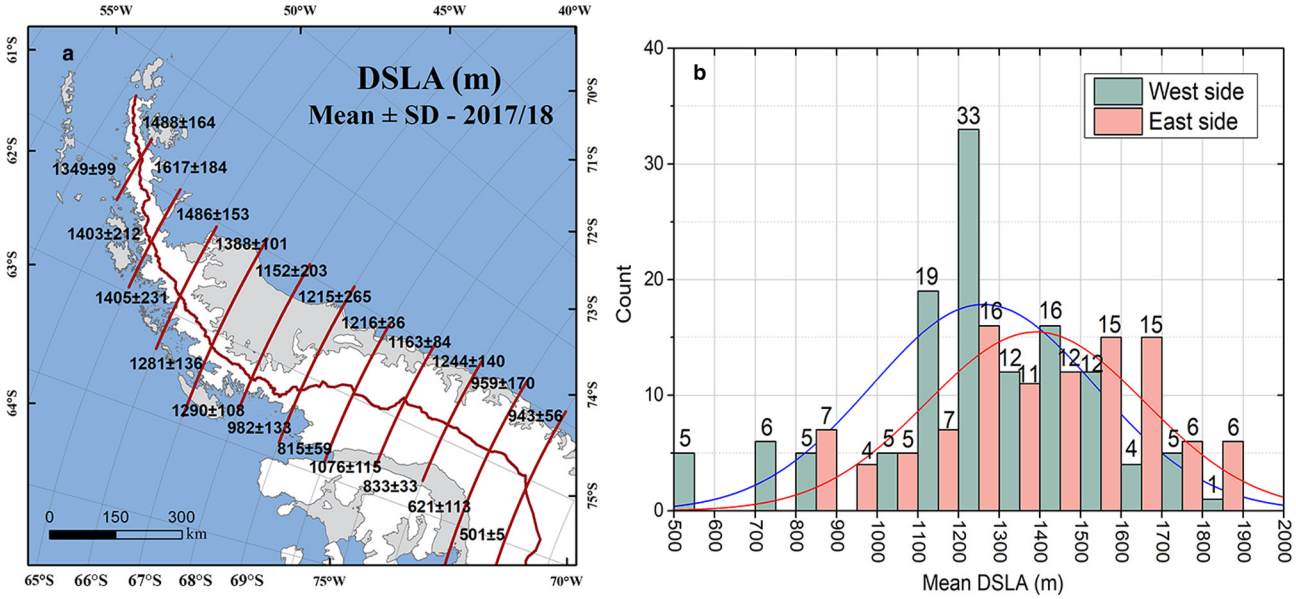

Fig. 4. Spatial distribution of mean values of DSLA. (a) Mean DSLA (in m) for different sectors divided by latitude on the AP for 2017/18. (b) Altitude histogram of glaciers in 2017/18. Red line in (a) shows the boundaries of the sectors used for analysis. Red and blue lines in (b) represent distribution curves of the west and east sides of the AP, respectively. Numbers in (b) indicate the number of glaciers for each range.

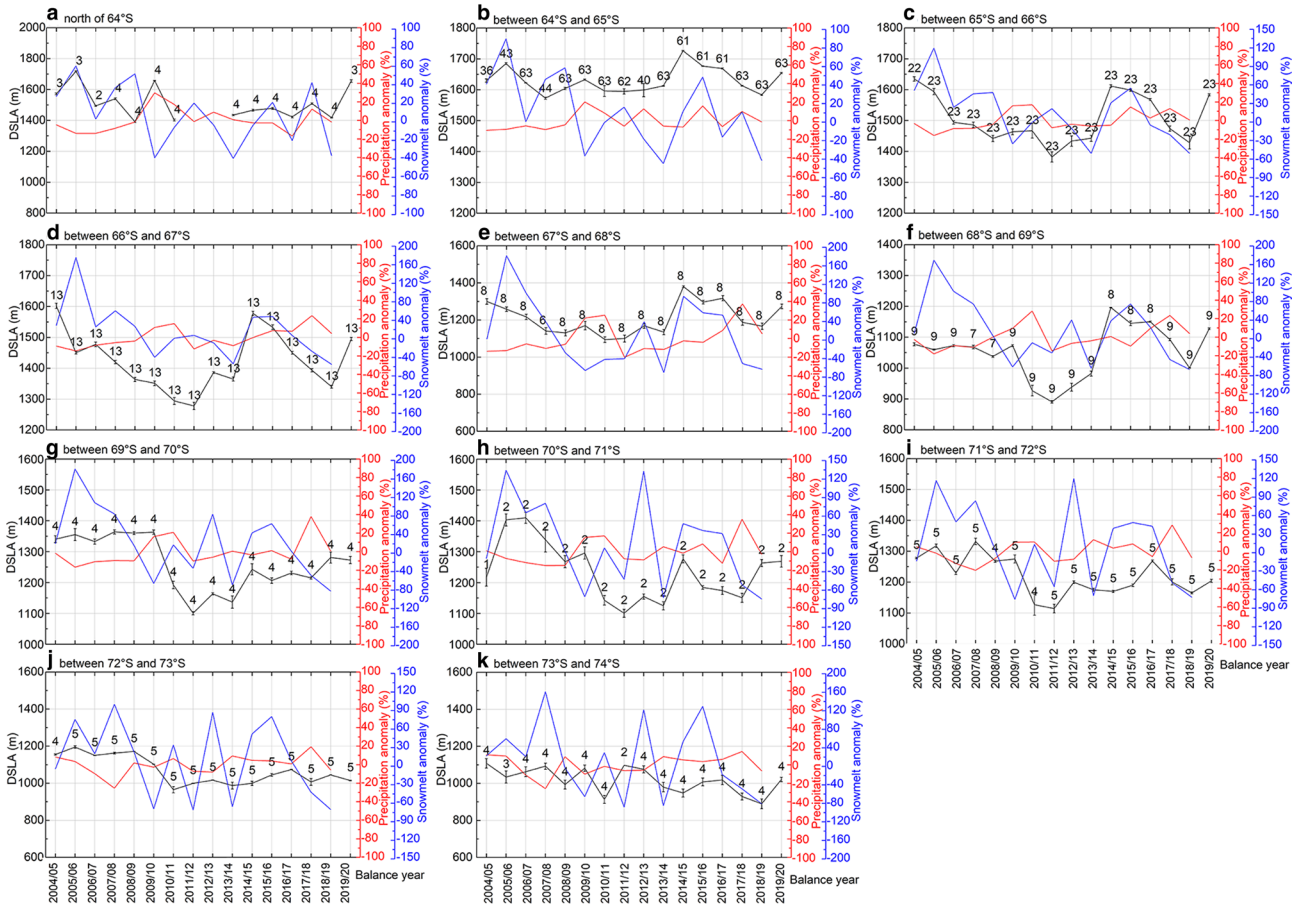

Fig. 5. Annual changes in the DSLA, precipitation anomalies and snowmelt anomalies in sectors along the east side of the AP. Numbers indicate the sample size of glaciers for each period. Error bars represent standard errors of the DSLA, which are calculated by dividing the std dev. by the sample size of glaciers.

higher on the west side because the temperature is lower on the east side at the same latitudes. However, the RACMO model between 2004/05 and 2018/19 indicated that the average snowmelt is relatively similar on both the west and east sides of the AP (Fig. S3a), but the average precipitation on the west side of the AP is significantly higher than the east side (Fig. S3b). Precipitation is over 3000 mm w.e. on the west coast and <500 mm w.e. on the east coast (van Wessem and others, 2016). On the east side of the AP, the amount of snowmelt often exceeds the amount of precipitation (van Wessem and others, 2016). The

https://doi.org/10.1017/jog.2021.72 Published online by Cambridge University Press

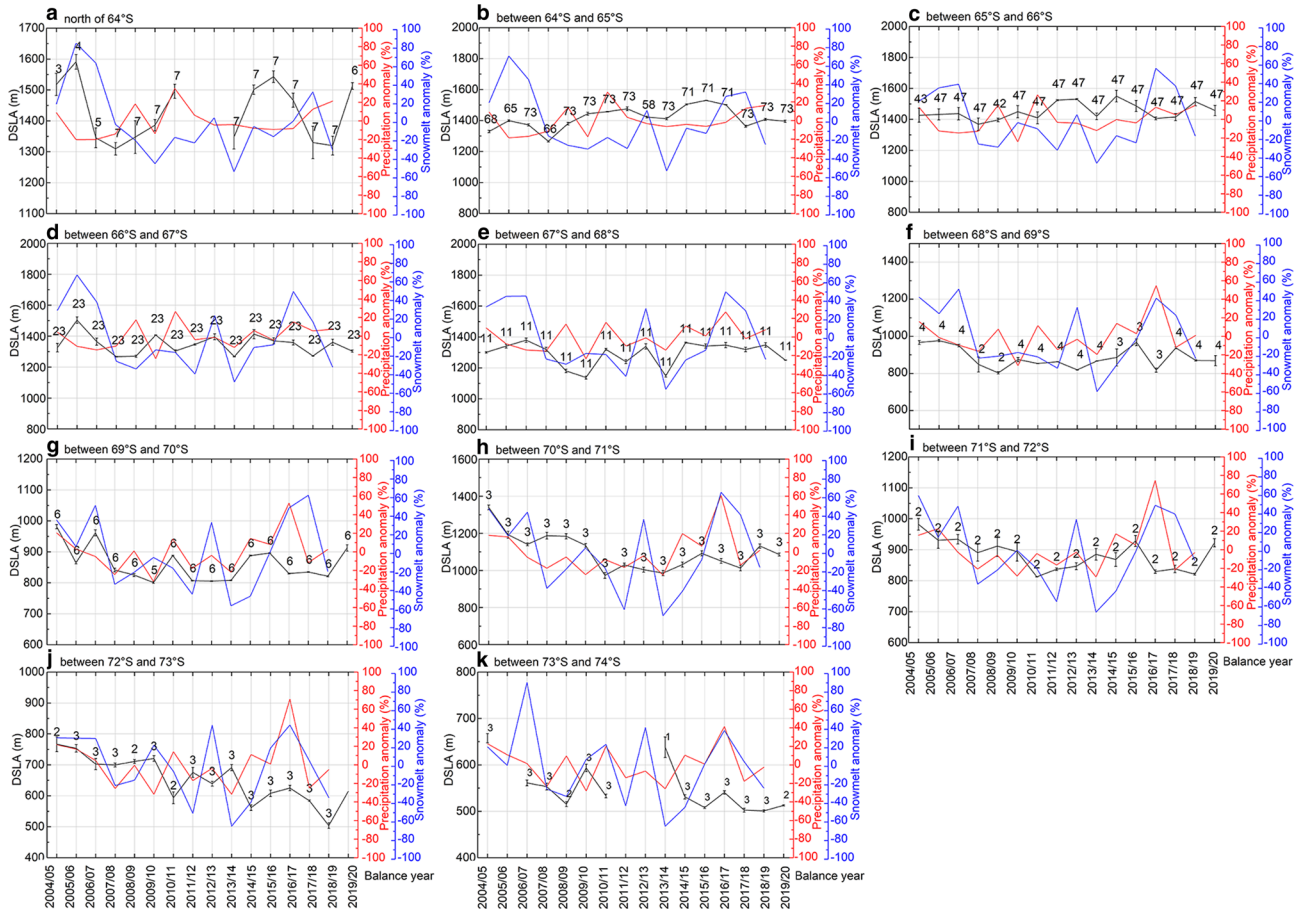

Fig. 6. Annual changes in the DSLA, precipitation anomalies and snowmelt anomalies in sectors along the west side of the AP. Numbers indicate the sample size of glaciers for each period. Error bars represent standard errors of the DSLA, which are calculated by dividing the std dev. by the sample size of glaciers.

Table 2. Total annual precipitation, total annual snowmelt (in mm w.e. (snow water equivalent)) and changes in DSLA on the east side of the AP from 2004/05 to 2018/19

Sector	Mean total annual precipitation and std dev. ($\times 10^5$ mm w.e.)	Mean total annual snowmelt and std dev. ($\times 10^3$ mm w.e.)	Trend in total annual precipitation (%/a)	Trend in total annual snowmelt (%/a)	Trend in DSLA (m/a)
North of 64°S	0.51 ± 0.06	14.13 ± 4.30	0.42	−3.21	−10.98
64°S/65°S	2.96 ± 0.30	60.74 ± 22.12	0.79	−4.64*	0.79
65°S/66°S	1.66 ± 0.17	36.88 ± 15.53	1.01	−6.26**	−3.25
66°S/67°S	1.83 ± 0.20	21.57 ± 10.95	1.45*	−6.87*	−3.91
67°S/68°S	1.18 ± 0.19	2.43 ± 1.59	1.58	−5.62	1.85
68°S/69°S	2.33 ± 0.31	7.50 ± 4.44	1.19	−7.43*	2.36
69°S/70°S	1.71 ± 0.25	5.42 ± 3.46	1.29	−9.15*	−11.54*
70°S/71°S	1.57 ± 0.22	4.07 ± 2.48	1.11	−5.95	−11.76*
71°S/72°S	1.65 ± 0.21	3.35 ± 1.99	0.97	−4.84	−8.16*
72°S/73°S	1.71 ± 0.18	2.82 ± 1.56	0.67	−4.13	−12.32
73°S/74°S	1.69 ± 0.18	1.39 ± 0.96	0.47	−5.26	−10.36

* and ** indicate the trend that is statistically significant at the 95 and 99% level, respectively.

total annual SMB demonstrates that the net accumulation on the west side is much higher than that of the other side (Fig. 9), which supports our result.

Responses of DSLA to climate show different patterns on both sides of the AP. Snowmelt becomes the main factor that dominates DSLA variations on the east side where precipitation is low. Changes in DSLA on the east side between 64°S and 69°S are consistent with variability in snowmelt from 2013/14 to 2018/19 (Figs 5b–f). This logarithmic total annual snowmelt–DSLA relationship provides an important link between total annual snowmelt and DSLA. As the total annual snowmelt rises, DSLA rises rapidly, and then the rate of increase slows down because of the low temperature limitation at high altitudes. DSLA is more influenced by the combination of precipitation and snowmelt on the west side; hence, R^2 of the total annual snowmelt–DSLA fit on the west side is less than the east side. Interestingly, higher total annual precipitation does not lead to the lower DSLA. DSLA begins to rise when the total annual precipitation exceeds $\sim 5 \times 10^5$ mm w.e., which can be explained by the atmosphere being warm and wet in areas with increased precipitation (mainly in the northwestern region of AP) and therefore accompanied by increased snowmelt. Snowmelt plays an

https://doi.org/10.1017/jog.2021.72 Published online by Cambridge University Press

Table 3. Total annual precipitation, total annual snowmelt and changes in DSLA on the west side of the AP from 2004/05 to 2018/19

Sector	Mean total annual precipitation and std dev. ($\times10^5$ mm w.e.)	Mean total annual snowmelt and std dev. ($\times10^3$ mm w.e.)	Trend in total annual precipitation (%/a)	Trend in total annual snowmelt (%/a)	Trend in DSLA (m/a)
North of 64°S	2.37 ± 0.39	4.48 ± 1.69	0.95	−3.51	−3.94
64°S/65°S	12.00 ± 1.71	26.38 ± 8.87	0.97	−2.11	8.20*
65°S/66°S	99.94 ± 1.42	17.93 ± 5.58	0.87	−0.70	−0.34
66°S/67°S	11.66 ± 1.59	19.32 ± 6.82	0.93	−2.01	−2.15
67°S/68°S	77.52 ± 1.10	24.30 ± 8.59	1.03	−1.58	2.15
68°S/69°S	48.36 ± 0.98	11.10 ± 3.77	0.92	−1.78	−3.18
69°S/70°S	61.36 ± 1.30	12.66 ± 4.89	0.89	−0.23	−5.80
70°S/71°S	28.80 ± 0.64	5.38 ± 2.24	0.75	−0.86	−14.61**
71°S/72°S	38.94 ± 1.02	6.26 ± 2.52	0.57	−1.22	−7.75**
72°S/73°S	43.51 ± 1.15	3.28 ± 1.17	0.04	−1.99	−14.54**
73°S/74°S	57.60 ± 1.14	2.05 ± 0.82	−0.26	−2.14	−6.34

* and ** indicate the trend that is statistically significant at the 95 and 99% level, respectively.

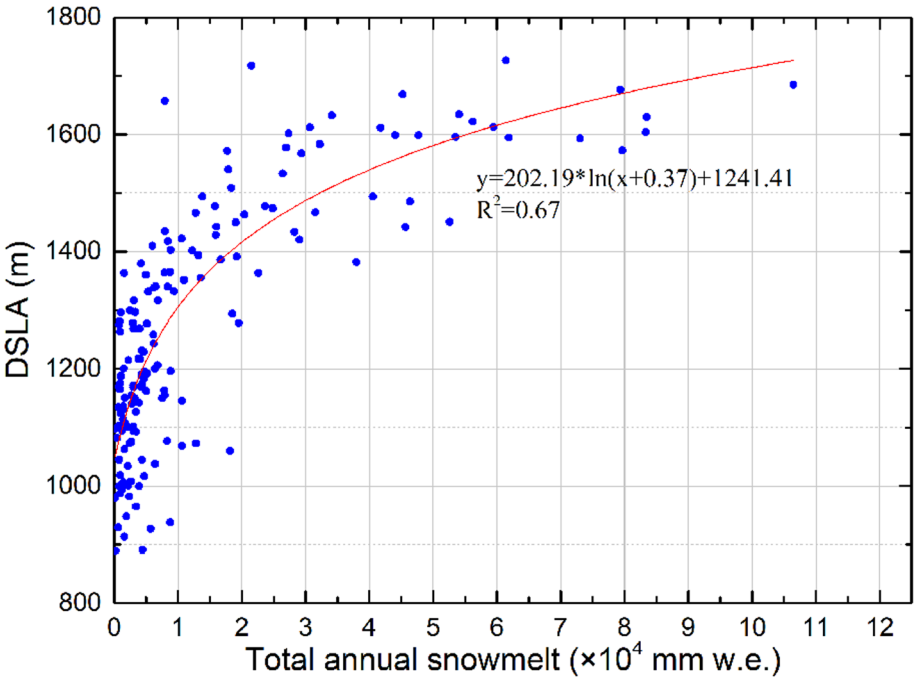

Fig. 7. Relationship between DSLA and total annual snowmelt on the east side of the AP. The solid line denotes the fitting curve. R^2 indicates the goodness of fit.

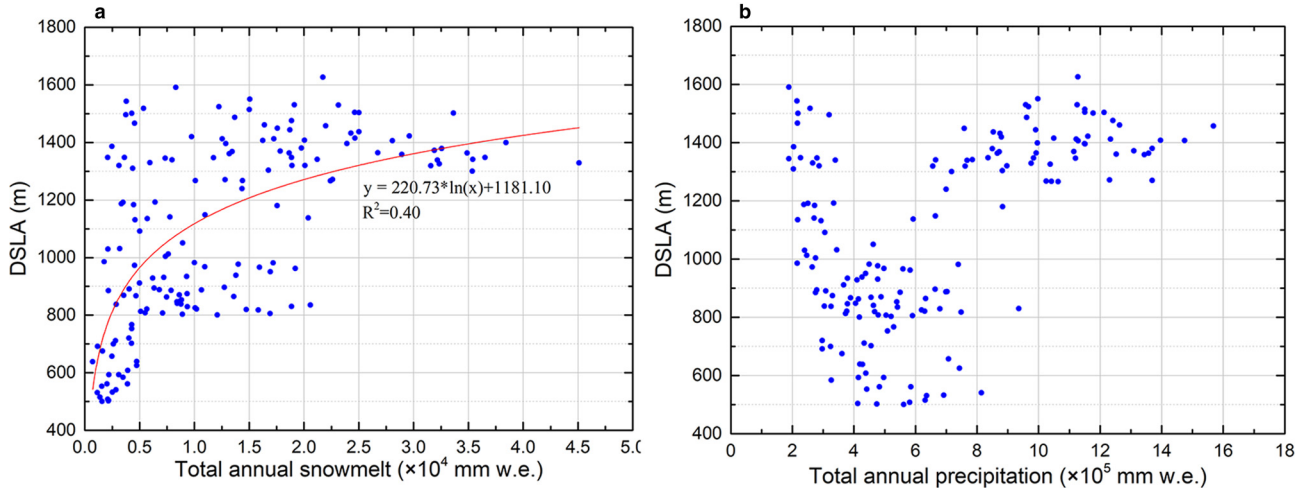

Fig. 8. Relationships between DSLA and (a) total annual snowmelt and (b) total annual precipitation on the west side of the AP. Solid line in (a) denotes the fitting curve. R^2 indicates the goodness of fit.

https://doi.org/10.1017/jog.2021.72 Published online by Cambridge University Press

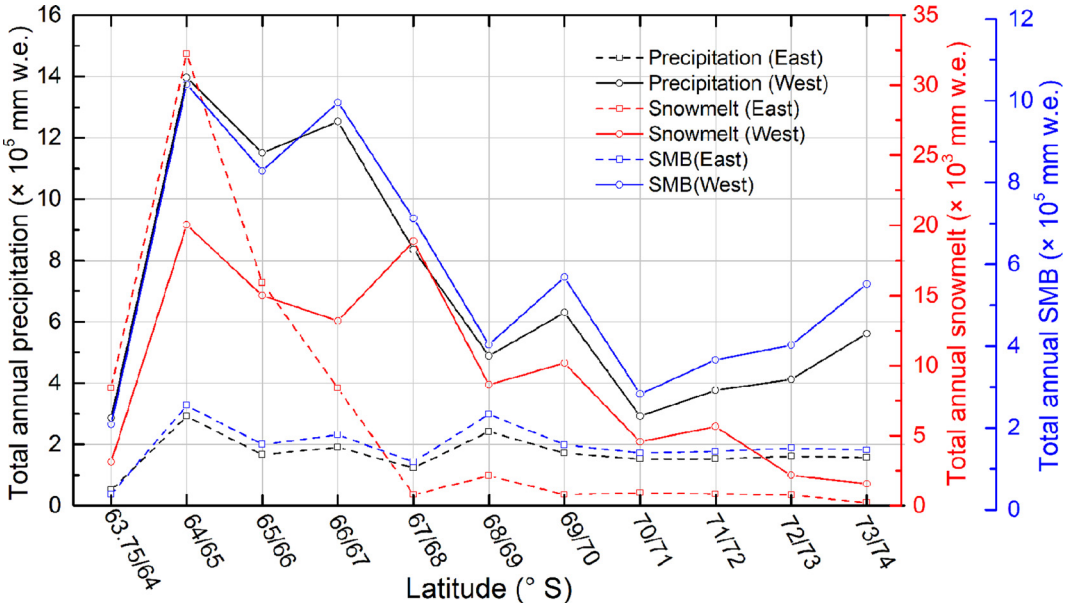

Fig. 9. Total annual precipitation, snowmelt and SMB on both sides of the AP in the balance year 2017/18.

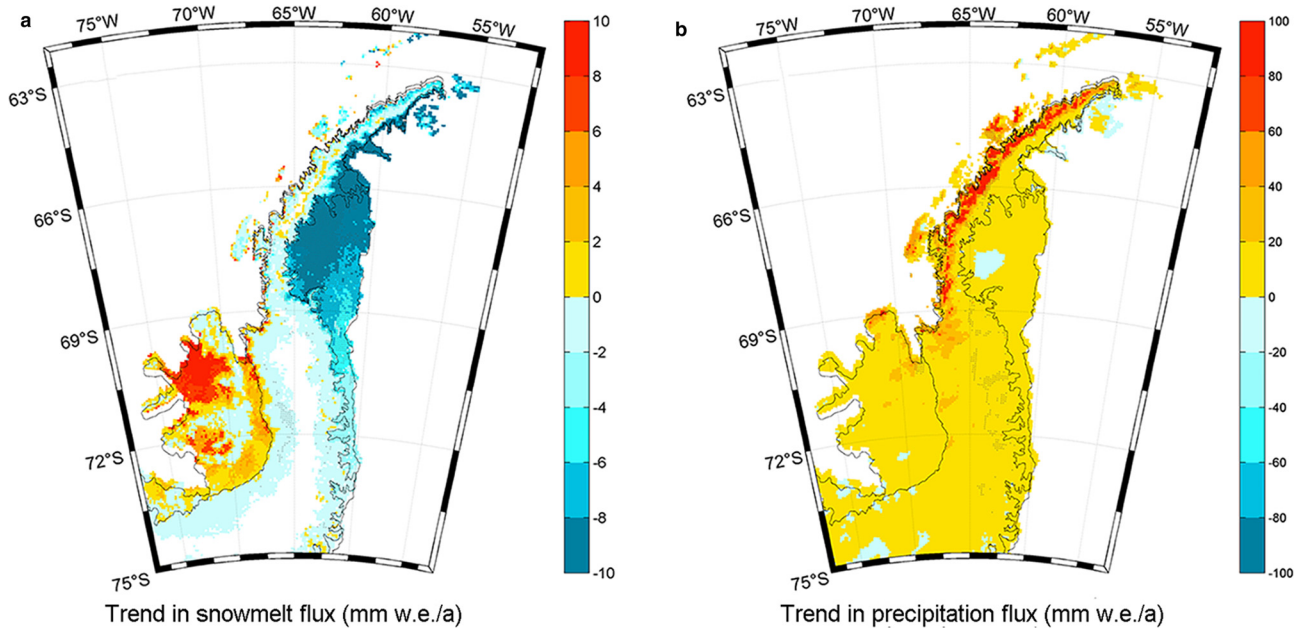

Fig. 10. Trends in the RACMO-based (a) snowmelt flux and (b) precipitation flux at each location on the AP between 2004/05 and 2018/2019. Shaded regions indicate the areas significant at 95% confidence level.

important role in changes of the DSLA, with precipitation not fluctuating to a large extent between 2004/05 and 2018/2019. Intense melting will likely increase the DSLA, while only the continuous accumulation of fine snow without melting metamorphism can migrate the DSL downwards. Therefore, the relationship between the DSLA and climate on the west side is more complicated than that on the east side.

5.2 Outlook and limitations

Climatic variables simulated by RACMO reveal increasing precipitation and decreasing snowmelt in most areas of the Graham Land and Palmer Land (Fig. 10). In response, DSLA in most sectors shows declining trends, especially on the southern AP. However, DSLA in sectors 68°S/69°S on the west side, and 64°S/65°S and 67°S/68°S on both sides show increasing trends. We speculate this is caused by increased snowmelt at high altitudes between 64°S and 69°S (Fig. 10a). Enhanced winter snowmelt on the AP may also be a factor in the increased DSLA (Zheng and others, 2020). However, the DSL in sectors 65°S/66°S and 66°S/67°S migrate downwards in the same climatic context as several of the regions mentioned above. Due to the lack of in situ measurements on the high parts of glaciers and the complex relationship between snowfall and snowmelt interactions, the quantitative relationship between DSLA and multivariate variables precipitation and snowmelt need to be further studied.

https://doi.org/10.1017/jog.2021.72 Published online by Cambridge University Press

Previous studies established a precedent for classifying glacier zones from SAR images (Rau and others, 2000*a*; Rau, 2002; Rau and Braun, 2002) and analysed the annual changes in some areas of the AP (Arigony-Neto and others, 2007, 2009). Compared with these studies, our analysis investigated the variations in the DSL on a larger scale based on a long time series.

Several limitations exist in our study. A constant backscattering threshold is unsuitable for all snowpacks on the AP given the different snowpack structures (e.g. snow depth, snow density and stratigraphy) in various areas of the AP. Moreover, SAR images orthorectified by the DEM with a low resolution lead to some uncertainties due to the complex terrain on the AP. A high-resolution DEM is necessary to improve the results, and dynamic thresholds applied to different sectors should be investigated further. Nevertheless, a quantitative analysis was conducted between DSLA and climatic variables rather than change monitoring alone. We also demonstrate that changes in DSLA can be used as a proxy of local climate and have the potential to validate reanalysis or climate model output in high-altitude areas with no in situ meteorological observations (Arigony-Neto and others, 2009).

6. Conclusions

Multitemporal C-band SAR images were analysed to explore spatiotemporal changes in the DSLA on the AP. The DSLA on the east side of the AP is generally higher than that on the west side, and the simulated SMB supports our result, showing higher net accumulation on the west side compared to the east side. The AP was reported to be the only area of Antarctica where widespread surface melt occurred (Abram and others, 2011). Extreme snowmelt has even impacted the central plateaus on the AP. The upward migration of the DSL in 2004/05, 2005/06 and 2012/13 is attributed to extreme snowmelt. Decreases in the DSLA in 2010/11 are the response to high positive precipitation anomalies and the absence of extreme snowmelt.

DSLA in most sectors shows declining trends, especially in the southern regions of the AP. This phenomenon can be interpreted as being caused by a decrease in snowmelt due to regional cooling (van Wessem and others, 2016; Zheng and others, 2019) and an increase in precipitation in recent years. A rise in the DSLA in northern sectors of AP is explained by an increase in snowmelt at high altitudes. Furthermore, the correlation between DSLA changes and simulated climatic variables on the AP was analysed. It demonstrates that the satellite-derived DSL can be an indicator of the local climate in the AP. With the increase in available SAR data and the support of a high-resolution DEM, DSLA could be used as an input to climate models to constrain the upper boundary of snowmelt.

Supplementary material. The supplementary material for this article can be found at https://doi.org/10.1017/jog.2021.72

Acknowledgements. The authors declare that they have no known competing financial interests or personal relationships that could have appeared to influence the work reported in this paper. The Reference Elevation Model of Antarctica digital surface model is available from the University of Minnesota (https://www.pgc.umn.edu/data/rema/). We acknowledge Dr J. M. van Wessem for providing the RACMO2.3 Antarctic Peninsula simulations. This work was supported by the National Natural Science Foundation of China (Grant Nos. 41776200, 41941010 and 41531069), and the Funds for the Distinguished Young Scientists of Hubei Province (China) (2019CFA057).

References

Abram NJ, Mulvaney R and Arrowsmith C (2011) Environmental signals in a highly resolved ice core from James Ross Island, Antarctica. *Journal of Geophysical Research Atmospheres* **116**(D20), D20116. doi: 10.1029/2011jd016147

Arigony-Neto J and 5 others (2006) Monitoring snow parameters on the Antarctic Peninsula using satellite data – a new methodological approach. *European Association of Remote Sensing Laboratories EARSeL eProceedings* **5**, 100–110.

Arigony-Neto J and 5 others (2007) A time series of SAR data for monitoring changes in boundaries of glacier zones on the Antarctic Peninsula. *Annals of Glaciology* **46**, 55–60. doi: 10.3189/172756407782871387

Arigony-Neto J and 6 others (2009) Spatial and temporal changes in dry-snow line altitude on the Antarctic Peninsula. *Climatic Change* **94**(1–2), 19–33. doi:10.1007/s10584-009-9550-1.

Benson C (1961) Stratigraphic studies in the snow and firn of the Greenland Ice Sheet. *SIPRE Res. Rep.* 70.

Bevan SL and 5 others (2018) Decline in surface melt duration on Larsen C ice shelf revealed by the advanced scatterometer (ASCAT). *Earth and Space Science* **5**(10), 578–591. doi: 10.1029/2018ea000421

Bindschadler R and 8 others (2008) The Landsat Image Mosaic of Antarctica. *Remote Sensing of Environment* **112**(12), 4214–4226. doi:10.1016/j.rse.2008.07.006.

Bromwich DH and Nicolas JP (2014) New reconstruction of Antarctic near-surface temperatures: multidecadal trends and reliability of global reanalyses. *Journal of Climate* **27**(21), 8070–8093. doi: 10.1175/jcli-d-13-00733.1

Costi J and 7 others (2018) Estimating surface melt and runoff on the Antarctic Peninsula using ERA-Interim reanalysis data. *Antarctic Science* **30**(6), 379–393. doi:10.1017/s0954102018000391.

Datta R and 5 others (2018) Melting over the northeast Antarctic Peninsula (1999–2009): evaluation of a high-resolution regional climate model. *The Cryosphere* **12**, 2901–2922. doi: 10.5194/tc-12-2901-2018

Dwyer C (2020) It was 65 degrees in Antarctica this week, National Public Radio. Available at https://www.npr.org/2020/02/21/808187601/-antarctica-melts-nasa-says-showing-effects-of-record-heat.

Ecmwf (2009) Part IV: physical processes. IFS Documentation CY33R1, ECMWF.

Gardner AS and 15 others (2013) A reconciled estimate of glacier contributions to sea level rise: 2003 to 2009. *Science (New York, N.Y.)* **340**(6134), 852–857. doi:10.1126/science.1234532.

Hock R, de Woul M, Radić V and Dyurgerov M (2009) Mountain glaciers and ice caps around Antarctica make a large sea-level rise contribution. *Geophysical Research Letters* **36**(7), L07501. doi: 10.1029/2008GL037020

Howat IM, Porter C, Smith BE, Noh MJ and Morin P (2019) The reference elevation model of Antarctica. *The Cryosphere* **13**(2), 665–674. doi: 10.5194/tc-13-665-2019

Hrbáček F, Láska K and Engel Z (2016) Effect of snow cover on the active-layer thermal regime – a case study from James Ross Island, Antarctic Peninsula. *Permafrost Periglacial Process* **27**(3), 307–315. doi: 10.1002/ppp.1871

Huang L and 5 others (2011) Classification and snow line detection for glacial areas using the polarimetric SAR image. *Remote Sensing of Environment* **115**(7), 1721–1732. doi: 10.1016/j.rse.2011.03.004

Huang L, Li Z, Tian B, Chen Q and Zhou J (2012) Comparison of different methods in glacier snow line detection using the polarimetric SAR image. *2012 Ieee International Geoscience and Remote Sensing Symposium*, Munich, German, 2012, 4426–4429.

Huang L, Li Z, Tian B, Chen Q and Zhou J (2013) Monitoring glacier zones and snow/firn line changes in the Qinghai–Tibetan Plateau using C-band SAR imagery. *Remote Sensing of Environment* **137**, 17–30. doi: 10.1016/j.rse.2013.05.016

Mladenova IE, Jackson TJ, Bindlish R and Hensley S (2013) Incidence angle normalization of radar backscatter data. *IEEE Transactions on Geoscience and Remote Sensing* **51**(3), 1791–1804. doi: 10.1109/TGRS.2012.2205264

Oliva M and 7 others (2017) Recent regional climate cooling on the Antarctic Peninsula and associated impacts on the cryosphere. *Science of the Total Environment* **580**, 210–223. doi:10.1016/j.scitotenv.2016.12.030.

Paterson W (1994) *Physics of Glaciers*, 3rd edn. Oxford: Butterworth-Heinemann.

Peel D (1992) Spatial temperature and accumulation rate variations in the Antarctic Peninsula. In Morris EM (ed.), *The Contribution of Antarctic Peninsula Ice to Sea Level Rise: Report for the Commission of the European Communities Project EPOC-CT90-0015*. Cambridge, British Antarctic Survey, pp. 11–15.

Proksch M and 6 others (2015) MEMLS3&a: microwave emission model of layered snowpacks adapted to include backscattering. *Geoscientific Model Development* **8**(3), 2605–2652. doi:10.5194/gmdd-8-2605-2015.

Rau F and 7 others (2000*a*) Monitoring multi-year snow cover dynamics on the Antarctic Peninsula using SAR imagery. *Polarforschung* **67**(1/2), 27–40.

Rau F (2002) The upward shift of dry snow line on the Northern Antarctic Peninsula Proc. of EARSel-LISSIG-Workshop Observing Cryosphere from Space, Bern.

Rau F and Braun M (2002) The regional distribution of the dry-snow zone on the Antarctic Peninsula north of 70° S. *Annals of Glaciology* **34**(1), 95–100. doi: 10.3189/172756402781817914

Rau F, Braun M, Friedrich M, Weber F and Goßmann H (2000*b*) Radar glacier zones and their boundaries as indicators of glacier mass balance and climatic variability Proceedings of the 2nd EARSeL Workshop-Special Interest Group Land Ice and Snow, pp. 317–327.

Sancho LG and 8 others (2017) Recent warming and cooling in the Antarctic Peninsula region has rapid and large effects on lichen vegetation. *Scientific Reports* **7**(1), 5689. doi:10.1038/s41598-017-05989-4.

Topouzelis K and Singha S (2016) Incidence angle normalization of wide swath SAR data for oceanographic applications. *Open Geosciences* **8**(1), 450–464. doi: 10.1515/geo-2016-0029

Turner J and 8 others (2005) Antarctic climate change during the last 50 years. *International Journal of Climatology* **25**(3), 279–294. doi:10.1002/joc.1130.

Turner J and 9 others (2016) Absence of 21st century warming on Antarctic Peninsula consistent with natural variability. *Nature*, **535**(7612), 411–415. doi:10.1038/nature18645.

Ulaby FT, Moore RK, Fung AK and Rasool SI (1983) Book-review – microwave remote sensing – active and passive. *Space Science Reviews* **35**, 295.

Undén P (2002) *HIRLAM-5 scientific documentation*. Norrkoping: Swedish Meteorology and Hydrology Institute.

van Wessem JM and 6 others (2015) Temperature and wind climate of the Antarctic Peninsula as simulated by a high-resolution regional atmospheric climate model. *Journal of Climate* **28**(18), 7306–7326. doi:10.1175/jcli-d-15-0060.1.

van Wessem JM and 10 others (2016) The modelled surface mass balance of the Antarctic Peninsula at 5.5 km horizontal resolution. *The Cryosphere* **10**(1), 271–285. doi:10.5194/tc-10-271-2016.

van Wessem JM and 18 others (2018) Modelling the climate and surface mass balance of polar ice sheets using RACMO2 – Part 2: Antarctica (1979–2016). *The Cryosphere* **12**(4), 1479–1498. doi:10.5194/tc-12-1479-2018.

Vaughan DG and 8 others (2003) Recent rapid regional climate warming on the Antarctic Peninsula. *Climatic Change* **60**(3), 243–274. doi:10.1023/A:1026021217991.

Zheng L, Zhou C and Liang Q (2019) Variations in Antarctic Peninsula snow liquid water during 1999–2017 revealed by merging radiometer, scatterometer and model estimations. *Remote Sensing of Environment* **232**, 111219. doi: 10.1016/j.rse.2019.111219

Zheng L, Zhou C and Wang K (2020) Enhanced winter snowmelt in the Antarctic Peninsula: automatic snowmelt identification from radar scatterometer. *Remote Sensing of Environment* **246**, 111835. doi: 10.1016/j.rse.2020.111835

Zhou C and Zheng L (2017) Mapping radar glacier zones and dry snow line in the Antarctic Peninsula using Sentinel-1 images. *Remote Sensing* **9**(11), 1171. doi: 10.3390/rs9111171

https://doi.org/10.1017/jog.2021.72 Published online by Cambridge University Press